Cancer & Metabolism

RESEARCH

Open Access

# Improved VPS4B O-GlcNAc modification triggers lipid droplets transferring from adipocytes to nasopharyngeal carcinoma cells

Haimeng Yin[1,2†], Ying Shan[1,2†], Qin Zhu[3†], Ling Yuan[1,2], Feng Ju[4], Yu Shi[5], Yumo Han[1,2], Rui Wu[1,2], Tian Xia[1,2], Kaiwen Zhang[1,2], Yiwen You[1,2*] and Bo You[1,2*]

## Abstract

**Background** The tumor microenvironment (TME) supplies critical metabolites that support cancer cell survival and progression. Adipocytes support tumor progression by secreting free fatty acids (FFAs) and adipokines; however, the role and mechanisms underlying lipid droplet (LD) release from adipocytes remain elusive.

**Methods** Using two nasopharyngeal carcinoma (NPC) cell lines and primary human pre-adipocytes (HPA), we evaluate the effect of LDs on cell growth, proliferation, colony formation, and migration. We also assess the roles of LD on the tumor progression in vivo. Using RNA-seq analysis, we elucidate the effect of hypoxic NPC cell-derived exosomes (H-exo) on the gene expression profile of adipocytes. By co-culture system, we investigated the effect of vacuolar protein sorting 4 homolog B (VPS4B)-annexin A5 (ANXA5) interaction on adipocyte LD maturity and release.

**Results** Herein, we report that LDs, rather than FFAs, are the primary lipid form transferred from adipocytes to NPC cells, enhancing cancer progression. NPC cells internalize LDs directly via macropinocytosis, while H-exo induces oxidative stress and membrane fluidity in adipocytes, leading to LD release. Transcriptomic and proteomic analyses reveal that VPS4B triggers LD release by interacting with ANXA5, and low LKB1 in H-exo enhances VPS4B O-linked N-acetylglucosamine (O-GlcNAc) modification through the inhibition of serine/threonine kinase 11 (STK11/LKB1)-AMP-activated protein kinase (AMPK) pathway and activation of the hexosamine biosynthesis pathway (HBP) flux.

**Conclusions** This study uncovers critical mechanisms of LD transfer in the TME, suggesting new therapeutic avenues in NPC.

**Keywords** Nasopharyngeal carcinoma (NPC), Exosomes, VPS4B, ANXA5, LD release, Metabolic symbiosis

†Haimeng Yin, Ying Shan and Qin Zhu contributed equally to this work.

*Correspondence:
Yiwen You
youyiwen_nantong@163.com
Bo You
Youbo19891014@163.com

Full list of author information is available at the end of the article

## Introduction

Nasopharyngeal carcinoma (NPC), originating from the nasopharyngeal epithelium, is prevalent in Southeast Asia, especially China [1], and often presents with advanced lymph node metastases at diagnosis, impacting patient quality of life [2]. Despite various NPC biomarkers being studied for their precision oncology potential, the mechanisms of NPC progression remain unclear.

Lipid metabolic reprogramming is considered a hallmark of NPC and increases the tumorigenic potential. Recently, evidences have revealed that, METTL14 promotes lipid synthesis and sustains NPC progression via enhancing m(6)A modification of ANKRD22 mRNA [3], protein C receptor maintains cancer stem cell properties via activating lipid synthesis in metastatic or recurrent NPC [4], the HILPDA-CLS1 axis-mediated lipidomic remodeling promotes NPC radioresistance by accelerating mitophagy [5]. Therefore, overseeing lipid metabolic reprogramming is important for upholding proper cell function and countering NPC expansion, metastasis, and resistance to therapy.

Lipid droplets (LDs) are energy-storing organelles that prevent lipotoxicity by storing excess lipids [6]. These organelles possess a hydrophobic core surrounded by a phospholipid monolayer embedded with proteins that mediate receptor-ligand interactions and signaling pathways [7]. LDs have emerged as promising cancer biomarkers [8] with high LD content linked to cancer stem cell populations [9]. Meanwhile, the established importance of LDs, as the most important functional organelles in adipose tissue, in tumors contrasts sharply with our limited knowledge of their molecular basis, which has long been confusing in the research on NPC pathogenesis. Based on a previous study, Epstein–Barr virus (EBV)-encoded latent membrane protein 1 (LMP1) promotes cell division by inducing lipogenesis in NPC [10]. EBV persistence is favored in adipose tissue near bone marrow metastatic NPC foci [11]. However, these studies did not consider the role of LDs in NPC progression.

While cancer research has predominantly focused on tumor-intrinsic lipid synthesis, LD accumulation can also be influenced by tumor microenvironment (TME) [12]. In colorectal cancer, cancer-specific FBXW7β mutations coupled with CSN6 inhibit fatty acid synthase (FASN) degradation, fostering lipogenesis [13]. Glioblastoma cells with CDKN2A deletions show diminished polyunsaturated fatty acid (PUFA) sequestration and elevated lipid peroxidation [14]. Exosomes also modify the TME [15], our previous work found hypoxic adipocyte-derived exosomes promote LD accumulation in NPC cells [16]. Adipocytes have been shown to release lipid-filled vesicles, potentially providing a direct lipid source [17], yet little research explores LD transfer from cancer-associated adipocytes (CAAs) to tumor cells [18]. Thus, we examined whether NPC cells benefit from stimulating LD release from adipocytes.

In this study, we identified vacuolar protein sorting 4 homolog B (VPS4B) as a key regulator of adipocyte LD release in the hypoxic NPC microenvironment. Mechanistically, VPS4B interacts with annexin A5 (ANXA5) via its ATPase domain to facilitate LD mature and release. Additionally, O-linked N-acetylglucosamine (O-GlcNAc) modification of VPS4B is enhanced to maintain VPS4B function by the suppressed serine/threonine kinase 11 (STK11/LKB1)-AMP-activated protein kinase (AMPK) pathway. Our findings suggest a novel therapeutic strategy targeting LD accumulation in NPC, providing new insights into potential treatment approaches.

## Materials and methods

### Cell culture

The CNE2 and C666-1 cell lines were gifted by the Sun Yat-Sen University Cancer Center and cultured in RPMI-1640 media (Gibco: C118775500BT) with 10% fetal bovine serum (Gibco: 10099141) and 1% penicillin/streptomycin (Gibco: 15140-122). Human pre-adipocytes (HPA) were purchased from ScienCell (cat. no.7220) and induced using a Human Adipose-Derived Mesenchymal Stem Cell Adipogenic Differentiation Kit (Cyagen: HUXMD-90031). The STR profile of CNE2 cell line was controlled before the use. Cells were grown at 37 °C with 5% $CO_2$. For hypoxia treatment, cells were cultured in 1% $O_2$ for 24 h. All experiments were conducted within five passages of the cell lines after thawing for recovery and were routinely tested for *Mycoplasma* contamination.

### Adipocytes vesicles isolation and labeling

Adipocytes were incubated with BODIPY (Thermo Fisher, D3922) and C12 (Thermo Fisher, D3835) at 37 °C for 1 h in the dark. Labeled adipocytes were incubated in a medium without serum at 37 °C (10^6 cells/mL). After 24 h, the CM was collected and centrifuged at 1200× *g* for 15 min. The resulting supernatant was passed through a 0.8-μm syringe filter (Sigma, CLS431221) and then concentrated via 100-kDa centrifuge filters (Millipore, UFC910008). The filtrated (< 100 kDa) and concentrated vesicle-enriched (> 100 kDa) media were used to co-culture with NPC cells for 4 h before imaging.

### Cell proliferation assay

For the colony formation assay, NPC cells were seeded into six-well plates at a density of 100 cells/well. Cells were stained with crystal violet after one week of incubation, and images were taken under a white plate for observation.

EdU staining was performed using the Cell-Light EdU Apollo 567 In Vitro Imaging Kit (RiboBio: C10310-1). NPC cells were counted and seeded at 5000 cells/ well

in the 96-well. After undergoing EdU labeling, cell fixation, and staining, the numbers of cells labeled with (red dots) or without (blue dots) were calculated. EdU incorporation (%) = EdU-positive cells (red dots)/ EdU-positive cells (red dots) + Hoechst-positive cells (blue dots).

#### Transwell

Transwell assays were conducted using Corning Transwell plates (24 well; 8 μm pores). NPC cells (10^4) in 200 μL of serum-free medium were seeded in the upper chambers, with 500 μL of medium containing 10% FBS added to the lower chambers. After 12–16 h of incubation, non-migrating or non-invading cells on the upper chamber surface were removed, while the remaining cells were fixed, stained, imaged and counted.

#### Scratch assay

NPC cells were seeded in a six-well plate and grown to a confluent monolayer. We calculated and analyzed the scratch areas without cells immediately after scratching and at the end of the assay (after 24 h) based on digital pictures.

#### LDs extraction experiment

Adipocytes were incubated with BODIPY (Thermo Fisher, D3922) and C12 (Thermo Fisher, D3835) at 37 °C for 1 h in the dark. LDs were extracted using a Lipid Droplet Isolation Kit (ab242290; Abcam).

#### Exosome isolation and uptake

Exosomes were purified from the conditioned medium (CM) of NPC cells using gradient centrifugation. After ultracentrifugation at 100,000 g for 90 min at 4℃, exosomes were suspended in PBS. The exosome sediment was stained with a 3% tungstic acid phosphate aqueous solution and fixed for transmission electron microscopy.

In the uptake experiment, exosomes were incubated with PKH-67 dye (Sigma-Aldrich: MIDI67) at 37 °C for 20 min, ultracentrifuged again, and then co-cultured with adipocytes. Nuclei were stained using Hoechst.

#### Quantification of LD levels in adipocyte supernatant

The TG content was quantified using a Triglyceride Assay Kit (ab65336; Abcam). When the inhibitors (10 μM of MSC1094308 or 18 μM of brefeldin A) were used for 4 h before exosomes, quantitative analysis of LDs in the CM was standardized by manually counting the number of labeled LDs in three images from each group.

#### Fluorescence recovery after photobleaching (FRAP) assay

Adipocyte phospholipid membranes were pre-labeled with C12. A high-intensity pulsed laser was used to irradiate the cell membrane in the same area for each group of cells, causing light quenching of fluorescent molecules in this area. Low-intensity laser scanning was used to detect and record the diffusion rate of non-quenched fluorescent molecules around the 60 s quenched area. The fluorescence recovery fraction was calculated as the fluorescence intensity at the end-time point normalized to that before bleaching.

#### Animal procedures

To detect the role of LDs in NPC progression in vivo, we established tumor xenograft models by implanting $2 \times 10^{\wedge 6}$ CNE2 or C666-1 cells subcutaneously on the backs of (4- to 5-week-old) nude mice. All experiments were approved by the Committee on Ethics of the Laboratory Animal Center of Nantong University (RDD number: S20230420-007).

In the experiment aimed to provide evidence for the role of LDs in NPC progression in vivo, one week after tumor inoculation, the mice were peritumorally injected with LDs and intraperitoneally injected with PBS/5-(N-ethyl-N-isopropyl) amiloride (EIPA) (0.25 mg/kg) every other day until the endpoint.

In the experiment aimed to determine the effect of LD uptake on tumor progression, mice were fed a high-fat diet (HFD) (60% of calories were from fat) or a chow diet for six weeks before being subcutaneously injected with NPC cells. When tumor volumes reached 50–100 $mm^3$, mice in the experimental groups were peritumorally injected with endocytic inhibitors (5 mg/kg chlorpromazine or 0.25 mg/kg EIPA) every other day.

In the experiment designed to confirm the ATPase role of VPS4B in NPC tumorigenesis, mice were fed an HFD for six weeks before being subcutaneously injected with NPC cells. Then, mice were peritumorally injected with exosomes (10 μg/100 μL PBS) from hypoxic and normoxic NPC cells and intraperitoneally injected with PBS/Brefeldin A (50 mg/kg) /MSC1094308 (50 mg/kg) every other day one week post–tumor inoculation.

#### Immunohistochemistry (IHC)

IHC for Ki67, hypoxia-inducible factor 1 subunit alpha (HIF-1α), perilipin 2 (PLIN2) and CK19 was performed as previously described [16]. Paraffin sections were deparaffinized, after antigen retrieval and block endogenous peroxidase, tissue sections were incubated with the primary antibody at 4℃ overnight. Then, tissues were counter-stained with diamine benzidine (DAB) and hematoxylin (Sigma) staining. The staining intensity A was divided into: 1, negative; 2, weakly positive; 3, moderately positive; 4, strongly positive. The dyeing area B was divided into: 1, 0-25%; 2, 26-50%; 3, 51-75%; 4, >75%. The staining score was defined as dyeing intensity area A × dyeing area B.

### RNA-seq and proteomic analysis

Mature adipocytes were co-cultured with exosomes derived from normoxic or hypoxic CNE2 cells for 24 h. Total RNA was extracted from each group and quantified. RNA-seq was performed, and the corresponding heatmap, Gene set enrichment analysis (GSEA), and Kyoto Encyclopedia of Genes and Genomes (KEGG) analysis were visualized by Bioprofile Technology Co., Ltd (Shanghai, China).

Adipocytes were pretreated with control or lentiviral vectors expressing VPS4B purchased from GENE (Shanghai, China). Co-IP assays were conducted using a Co-IP Kit (Thermo Fisher, 14321D), as previously described [19], and different species of IP and WB antibodies were used. BiotechPack Scientific (Beijing, China) performed the proteomic analysis of the IP samples.

### ROS

Intracellular ROS production in adipocytes was measured by a dihydroethidium probe kit (DHE, BestBio, Beijing, China). Adipocytes pretreated with exosomes from hypoxic and normoxic NPC cells were digested with trypsin and resuspended in 500 μL PBS, probes were added and incubated for 1 h at 37 °C in the dark, and 480–535 nm wavelength excitation was used to detect cellular ROS content.

### $NADP^+$/NADPH assay

Regarding the $NADP^+$/NADPH assay kit (KA1663, Abnova), 40μL $NADP^+$/NADPH standards or cell samples were added into wells of a clear bottom 96-well plate. After incubating at RT for 20 min, 80μL working reagent was added quickly. After tapping plate to mix liquid briefly and thoroughly, the values of OD0 (optical density at time "zero") and OD30 (optical density for 30-min incubation at RT) were recorded at 565 nm. $NADP^+$ and NADPH concentrations were calculated from two separate standard curves.

### Immunofluorescence (IF) assay

HPA cells were seeded in 24-well plates with cell-climbing slices. After the induction, adipocytes were fixed with 4% paraformaldehyde for 15 min at RT and permeabilized with 0.5% Triton X-100/PBS for 10 min. The sections were blocked with 5% normal goat serum for 1 h at RT, and incubated overnight at 4 °C with VPS4B and ANXA5 antibodies from different species.

### AI drug screening and molecular Docking experiments

Based on the RNA-seq data, we identified 551 genes with high expression (log2FoldChange > 1) and 731 genes with low expression (log2FoldChange < -1). The Connectivity Map database (https://clue.io/) was queried to identify potential small-molecule compounds that can reverse global gene expression changes. The query parameter was set to Gene expression (L1000). Dicumaral and buflomedil were screened as NADPH inhibitors to reverse NADPH/$NADP^+$ ratio. The molecular structures of dicumarol and buflomedil were obtained from PubChem (https://pubchem.ncbi.nlm.nih.gov/). The three-dimensional (3D) coordinates of proteins VKORC1 (ID: Q9BQB6), NQO1 (ID: P15559), CRYZ (ID: Q08257), ADRAA (ID: P35348), and CACNA1C (ID: Q13936) were downloaded from UniProt (https://www.uniprot.org). Visualization of the model was performed using PyMOL 2.5.8 (https://pymol.org/2/) with default parameters.

### Cell transfection

Cells were transiently transfected by the lipofectamine 3000 kit. The HA-tagged full-length and truncated VPS4B plasmids were designed and synthesized by Azenta Life Sciences (Suzhou, China). Flag-tagged ANXA5 plasmid was purchased from GENE (Shanghai, China). ShLKB1 (5′-CCGGCATCTACACTCAGGACTTCACCTCGAG-GTGAAGTCCTGAGTGTAGATGTTTTTG-3′).

### Western blots

Western blotting was performed as previously described [19]. In brief, the lysates were denatured for 10 min at 100 °C, separated in 10% polyacrylamide gels, and transferred to PVDF blotting membranes. Membranes were blocked in 5% nonfat milk and incubated with primary antibodies overnight at 4 °C and secondary antibodies for 1 h at RT. Band signals were visualized by enhanced chemiluminescence (Thermo,32106). The following primary antibodies were used: anti-ALIX (Abcam; ab275377, 1:1000), anti-TSG101 (Abcam; ab133586, 1:1000), anti-CD63 (Proteintech Group; 25682-1-AP, 1:400), anti-CD9 (Abcam; ab236630, 1:1000), anti-actinin 4 (Abcam; ab227166, 1:1000), anti-flotillin 1 (Abcam; ab133497, 1:10000), anti-VPS4B (Proteintech Group; 17673-1-AP, 1:500), anti-ANXA5 (Proteintech Group; 11060-1-AP, 1:2000), anti-ANXA4 (Abclonal; A9203, 1:1000), anti-ANXA6 (Abclonal; A18069, 1:1000), anti-ANXA7 (Abclonal; A3733, 1:1000), anti-ANXA11 (Abclonal; A20841, 1:1000), anti-Flag (Beyotime; AF2852, 1:1000), anti-HA (Beyotime; AF0039, 1:1000), anti-LKB1 (Abclonal; A22636, 1:1000), anti-O-GlcNAc (Thermo Fisher; MA1-072, 1:1000), anti-GFAT (Proteintech Group; 14132-1-AP, 1:1000), anti-P-GFAT (IBL; 28123, 1:2000), anti-AMPK (Proteintech Group; 10929-2-AP, 1:1000), anti-P-AMPK (Sangon Biotech; D151212, 1:500), and anti-ACTB (Proteintech Group; 81115-1-RR, 1:5000).

### Statistical analysis and reproducibility

Except for RNA-seq, all statistical analyses were performed using GraphPad Prism software. Data are presented as the means ± standard error of the mean (s.e.m.) across triplicate experiments at two independent times to ensure consistency of the results. Data were compared between two groups using an unpaired two-tailed t-test. Survival curves were analyzed using the Kaplan–Meier log-rank test. Correlations between variables were assessed using Pearson's correlation coefficients. All results with a $P<0.05$ were considered statistically significant.

## Results

### Adipocyte-derived LDs promote the malignant biological behavior of NPC cells

It is reported that lung-infiltrating neutrophils transfer their stored LDs rather than free fatty acids (FFAs) to metastatic tumor cells, fueling breast cancer lung metastasis [18], which triggered us to investigate the role of LDs in NPC progression. In this study, we used 100-kDa centrifuge filters to divide C12 and BODIPY fluorescent lipid-labeled adipocyte CM into two fractions: one containing large particles, such as LDs and macromolecular proteins, and the other containing small particles, such as FFAs and the majority of soluble proteins. The experimental design is shown in Fig. 1A. Upon incubation of these two CM portions with CNE2 cells, the large CM portion was determined to be the primary contributor of lipids to tumor cells (Fig. 1B, C). Thus, NPC cells are likely to uptake lipids primarily through the form of LD. We quantified the content of LDs in co-cultured NPC cells and found that tumor cells can uptake LDs (Fig. S1A). Next, we investigated how NPC cell behavior changed after the internalization of LDs purified from adipocytes. NPC cell proliferation (Fig. 1D, E) and migration (Fig. 1F–I) were enhanced after co-culturing with LDs. Therefore, LDs can be transferred from adipocytes to NPC cells, allowing them to migrate and proliferate under nutrient-deprivation stress. Interestingly, C666-1 cells appear to have a greater ability to migrate than CNE-2 cells, which might be linked to the higher quantity of LDs in C666-1 compared to the CNE-2 cell line.

### NPC cells uptake adipocyte LDs mainly via macropinocytosis in hypoxia

To elucidate the mechanism of LDs internalization by NPC cells, we performed an in vitro simulation experiment (Fig. 2A). Adipocytes were stained with BODIPY, and fluorescently labeled LDs were collected and co-cultured with CNE2 cells. Three common endocytosis inhibitors were used to block LD absorption by CNE2 cells. Thus, the inhibition of macropinocytosis with EIPA had a stronger suppressive effect than the inhibition of clathrin-dependent endocytosis with chlorpromazine or caveolae-dependent endocytosis with genistein (Fig. 2B, C). The addition of EIPA reversed the LD-promoted NPC cell proliferation (Fig. 2D, E). Furthermore, tumor xenograft models in nude mice demonstrated a similar inhibitory role of EIPA in stabilizing tumor growth caused by adipocyte-derived LDs (Fig. 2F–J and Fig. S1B-E). Therefore, macropinocytosis is considered to be the principal LD-uptake method for NPC cells.

A HFD mouse model was used to simulate in vivo LD accumulation (Fig. 2K). The injection of chlorpromazine and EIPA to inhibit macropinocytosis and caveolae-dependent endocytosis resulted in the drastic arrest of HFD-induced tumor growth (Fig. 2L, M and Fig. S1F, G). In the present study, EIPA considerably inhibited tumor progression. This may be due to the fact that a HFD not only allows NPC cells to uptake LDs but also promotes tumor cell self-renewal, such as enhanced metabolic reprogramming. Immunostaining of tumor tissues showed a close correlation between *HIF-1α* and *PLIN2*, an important LD-associated protein (Fig. 2N, O and Fig. S1H, I), which means that there may be a positive correlation between LD infiltration and hypoxic TME.

Next, we explored the effects of LD infiltration in human tumors by analysing datasets. Given that HIF-2α/PLIN2 dependent lipid storage protects clear cell renal cell carcinoma cells against pharmacological ER stress under oxygen limitation [20], we investigated the prognoses of patients with head and neck squamous cell carcinoma (HNSC) overexpressing both *PLIN2* and *HIF-1α* using data from The Cancer Genome Atlas (TCGA). Fig. S1J shows that the combination of high expression of *HIF-1α* and *PLIN2* predicts poor outcomes. The messenger RNA gene expression profiles for NPCs in the GSE61218 dataset show that *PLIN2* expression correlated positively with *HIF-1α* expression (Fig. S1K). Therefore, the hypoxia is a substantial factor for LD accumulation in vivo.

### Exosomes derived from hypoxic NPC cells stimulate LD release in adipocytes

The crucial functions of LDs in the TME include providing nutrition, regulating metabolism, and transmitting signals [6]. Studies have shown that adipocyte cytokines [21], hormones [22], apoptosis, and differentiation [23] can promote the release of FFAs. However, studies on the mechanisms of LD release are lacking. Exosomes may mediate interactions within the tumor ecosystem and affect phenotypic inter-tumoral heterogeneity [24]. We established an in vitro model to confirm the role of exosomes in metabolic symbiosis between adipocytes and NPC cells (Fig. 3A). We purified exosomes from normoxic and hypoxic NPC cells and identified them using marker proteins and electron microscopy (Fig. 3B, C).

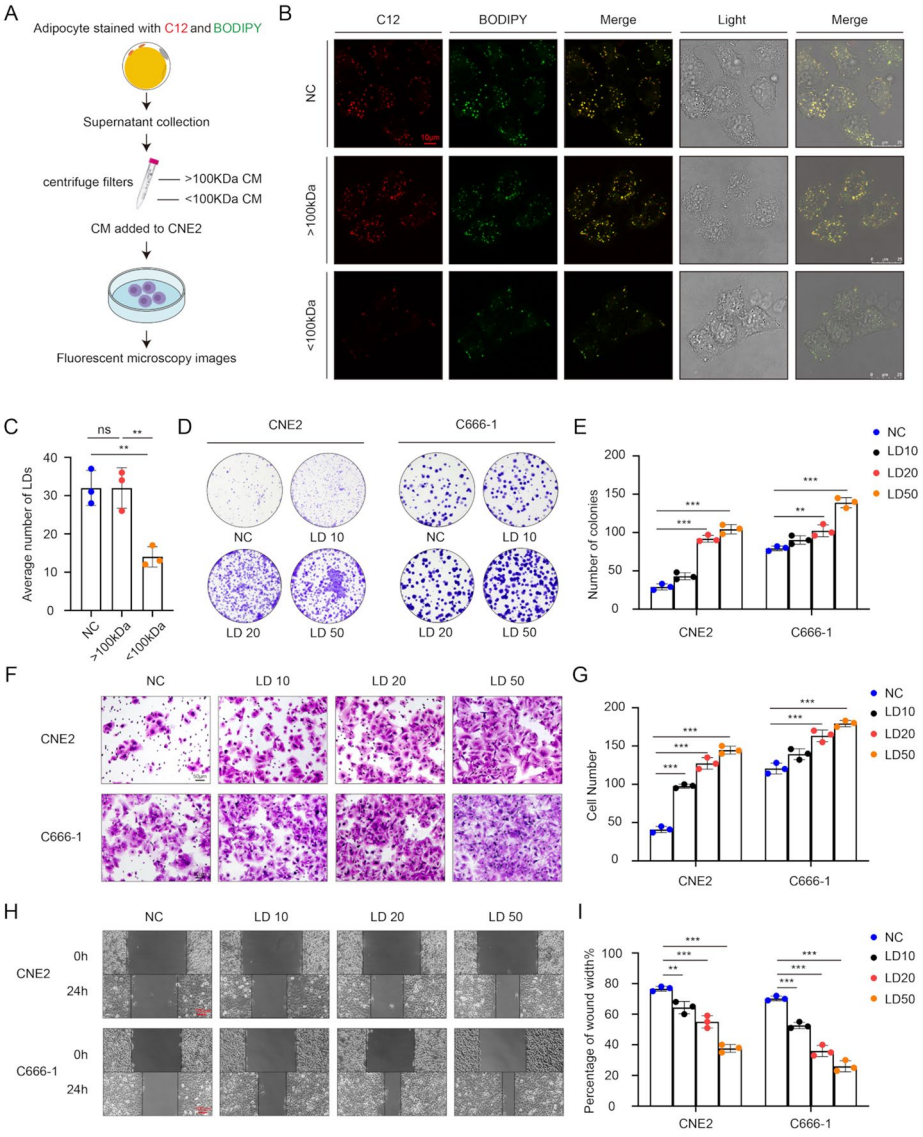


**Fig. 1** Adipocyte-derived LDs promote the malignant biological behavior of NPC cells. **(A)** Experimental design to identify the main form of lipids transfer from adipocytes to NPC cells: Adipocytes were stained with C12 and BODIPY to mark LDs. The supernatant of adipocytes was then collected and separated into small-sized (< 100 kDa) and large-sized (> 100 kDa) CM portions. The fluorescent microscopy images of CNE2 cells were collected after co-culture with filtrated CM for 4 h. **(B, C)** Representative images of LD internalization in CNE2 cells **(B)** and statistical chart **(C)**. NC, negative control. Scale bars, 10 μm. LD 10, LD 20, and LD 50 refer to LDs extracted from 10 mL, 20 mL, or 50 mL adipocyte supernatant, respectively. **(D, E)** Results of colony formation assay **(D)** and statistical chart **(E)** when LDs are added to CNE2 cells in a concentration-dependent manner. **(F–I)** Representative images of Transwell **(F)** and scratch assay **(H)** after adding LDs extracted from 10 mL, 20 mL, or 50 mL adipocyte supernatant to NPC cells. Scale bars, 100 μm. ns, not significant, $^{**}P < 0.01$, $^{***}P < 0.001$

The coculture experiments showed that hypoxic NPC cell-derived exosome (H-exo) rather than normoxia NPC cell-derived exosome (N-exo) facilitates the progress of adipocyte LD release (Fig. 3D, E). As expected, quantitative analysis of triglycerides (TGs) and LDs fluorescently pre-labeled with C12 in the adipocyte supernatant showed that the H-exo concentration gradient affected adipocyte LD release (Fig. 3F–I). Next, we developed a model to observe the ability of NPC cells to absorb LDs (Fig. 3J), and found that CNE2 cells exhibited increased LD absorption in the adipocyte-conditioned supernatant pretreated with H-exo (Fig. 3K, L). Therefore, we speculate that exosomes released by hypoxic NPC cells cause adipocytes to release LDs, which are then absorbed by NPC cells for reuse.

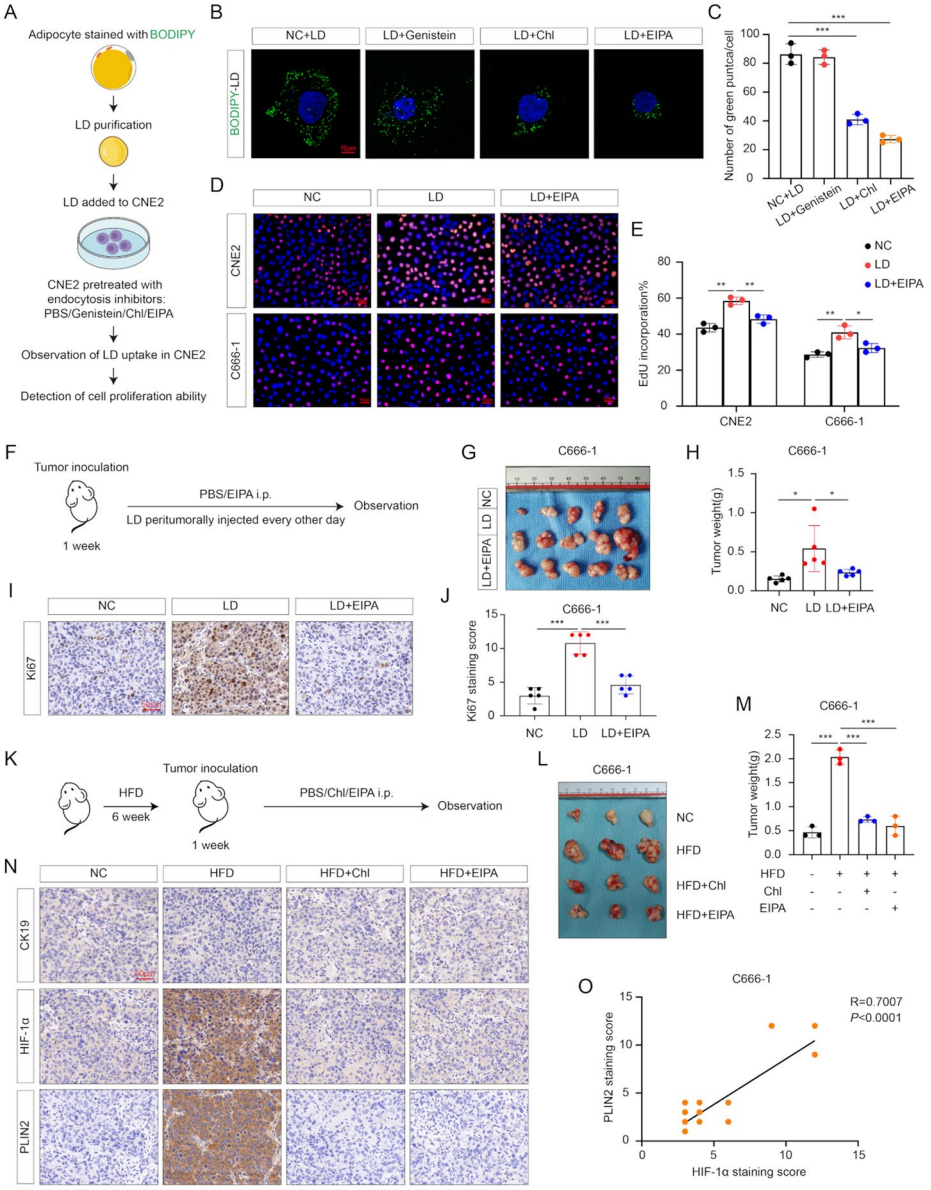


**Fig. 2** NPC cells uptake adipocyte LDs mainly via macropinocytosis in hypoxia. **(A)** Schematic of experimental approach used to detect the main endocytosis LD pattern in CNE2 cells. **(B, C)** The effects of chlorpromazine, genistein, and EIPA in blockage of LD internalization of NPC cells (chlorpromazine: clathrin-dependent endocytosis inhibitor; genistein: caveolae-dependent endocytosis inhibitor; EIPA: macropinocytosis inhibitor). Scale bars, 10 μm. **(D, E)** NPC cells were pretreated with EIPA (20 μM) for 1 h, and representative images and quantification data of EdU assays after adding LDs in CNE2 and C666-1 cells for 24 h. **(F)** Schematic of nude mice subcutaneous tumor model. **(G)** Images of xenografts in nude mice injected with C666-1 cells. **(H)** The tumor weight of the three groups. **(I, J)** Representative images and quantification of Ki67 staining. Scale bars, 50 μm. **(K)** Schematic of HFD mice subcutaneous tumor model. **(L)** Images of xenografts in nude mice injected with C666-1 cells. **(M)** The tumor weight of the four groups. **(N)** Representative IHC images of CK19, HIF-1α, and PLIN2. Scale bars, 50 μm. **(O)** Pearson's correlation analysis of HIF-1α and PLIN2 according to IHC scores ($n = 12$). $^{*}P < 0.05$, $^{**}P < 0.01$, $^{***}P < 0.001$

### ATPase VPS4B participates in adipocyte LD release

Changes in the fluidity of the cell membrane are generally involved in the release of cellular contents [25]. The FRAP assay showed that the effects of hypoxic exosomes on the membrane fluidity of adipocytes were not immediate and occurred 6 h after incubation (Fig. 4A). To identify the key proteins that maintain optimal adipocyte membrane fluidity for LD release, we performed RNA-seq of adipocytes pretreated with N-exo and H-exo (Fig. 4B, C). GSEA revealed an enrichment of the hypoxia signal and a reduction in oxidative phosphorylation in adipocytes with exposure to H-exo (Fig. S2A, B). This is in agreement with a previous study showing that hypoxia reprograms the metabolic mode of tumor cells

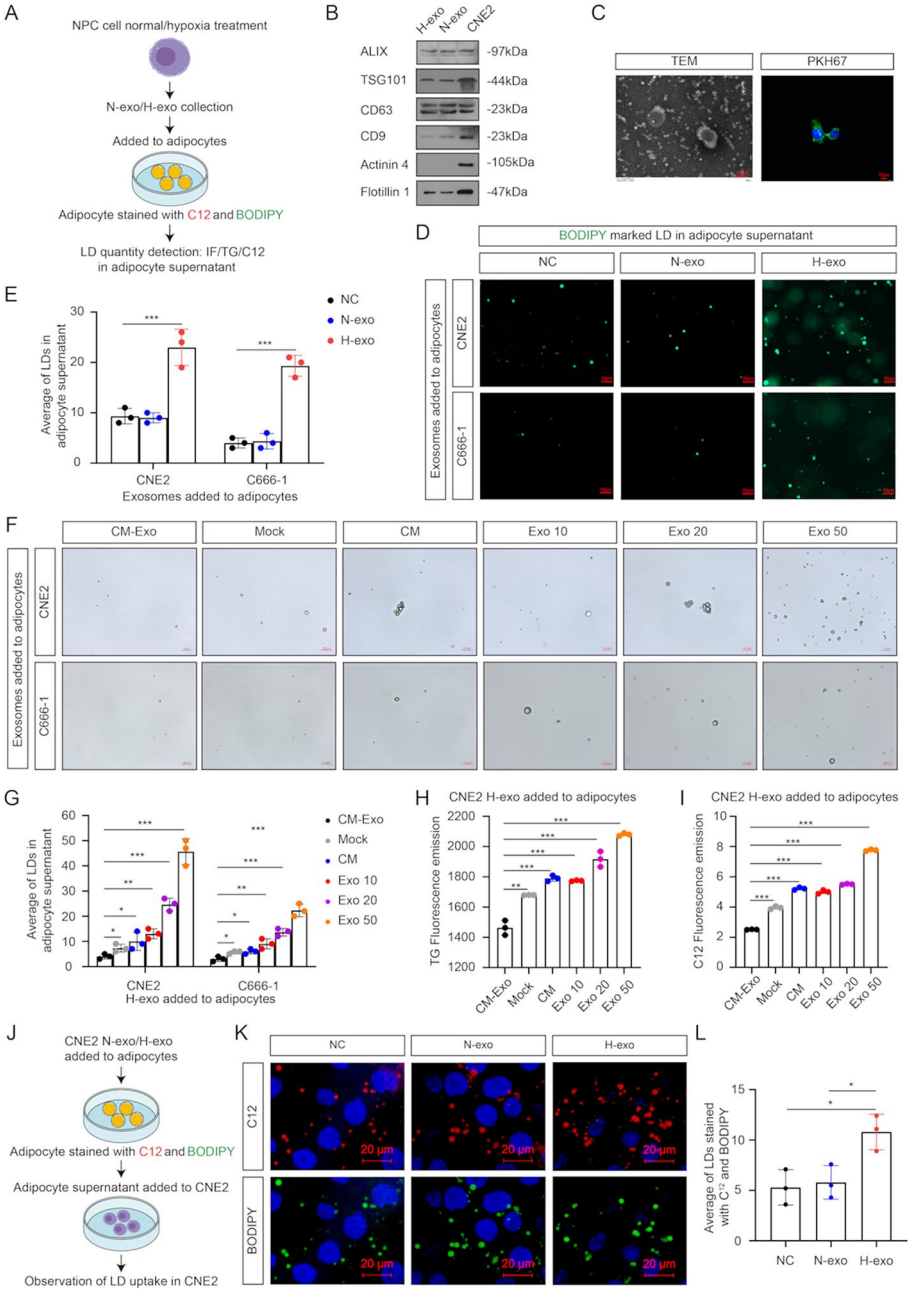


**Fig. 3** Exosomes derived from hypoxic NPC cells stimulate LD release in adipocytes. **(A)** Schematic of the in vitro adipocyte LD release experiments. **(B)** Western Blot analysis of ALIX, TSG101, CD63, CD9, Actinin 4, and Flotillin 1 in exosomes from normoxic and hypoxic CNE2 cells and CNE2 total proteins. **(C)** Electron micrographs of the cup-shaped vesicular structure of exosomes (scale bars, 100 nm) and the typical image of exosomes ingested by adipocytes (scale bars, 10 μm). **(D, E)** The addition of exosomes derived from CNE2 cells in normoxic and hypoxic conditions affected the LD release in adipocytes supernatant. Live adipocytes were stained with BODIPY (2 μM) at 37 °C for 1 h. Then, exosomes derived from NPC cells were added to adipocytes and incubated for 24 h. LDs in adipocyte supernatant were microscopically observed **(D)** and quantitatively analyzed **(E)**. Scale bars, 50 μm. **(F–I)** Typical images of LDs **(F)**, relevant density quantification **(G)**, analysis of TG content **(H)**, and fluorescence detection of C12-labeled LDs **(I)** after co-culturing with exosomes from hypoxic NPC cells in a dose-dependent manner (CM-Exo: NPC cell culture medium without exosomes; Mock: EBSS group; CM: NPC cell culture medium for 24 h; Exo: exosomes; Exo 10, 20, 50 refers to exosomes extracted from 10 mL, 20 mL or 50 mL NPC cell supernatant, respectively). Scale bars, 50 μm. **(J)** Schematic of the model for NPC cell uptake LDs. **(K, L)** Typical images of CNE2 cells uptake of LDs and relevant LD density quantification. Scale bars, 20 μm. $^{*}P < 0.05$, $^{**}P < 0.01$, $^{***}P < 0.001$

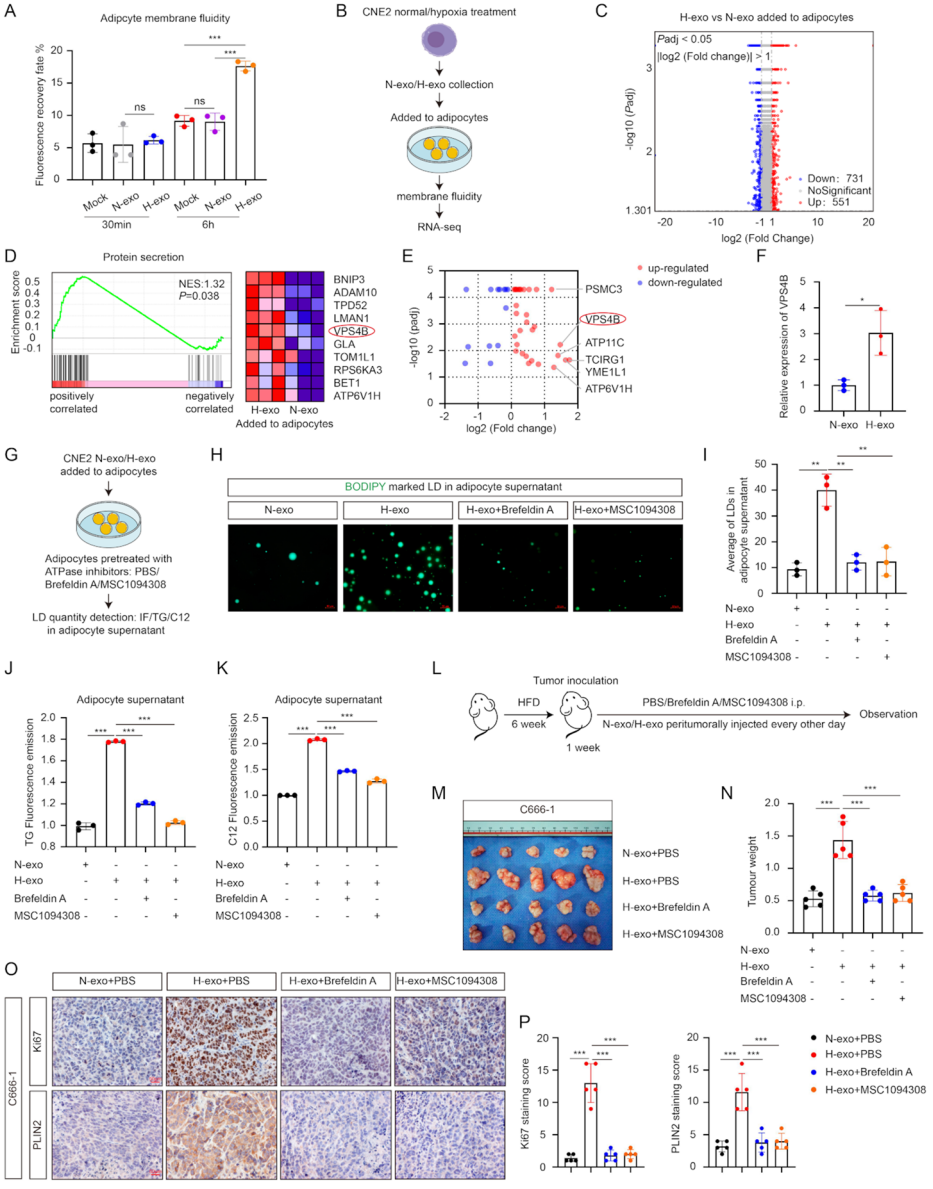


**Fig. 4** ATPase VPS4B participates in adipocyte LD release. **(A)** Changes in adipocyte membrane fluidity after the addition of exosomes derived from normoxic and hypoxic CNE2 cells. **(B)** Schematic of adipocyte membrane fluidity detection and RNA-seq. Specifically, adipocytes were treated with exosomes derived from normoxic and hypoxic CNE2 cells. Then, the RNA-seq of the two groups of adipocytes was carried out. **(C)** The volcano plot of the differentially expressed genes in adipocyte RNA-seq data. **(D)** GSEA showed significant enrichment in secretion, and the top 10 proteins are demonstrated on the right. **(E)** The volcano plot revealed the differential expression of ATPase between the two groups of adipocytes with the addition of exosomes from normoxic and hypoxic CNE2 cells. **(F)** In adipocytes pretreated with normoxic and hypoxic CNE2 exosomes, levels of VPS4B mRNA were detected. **(G)** Schematic of the in vitro LD-release experiments. **(H, I)** Typical images of LDs in different adipocyte supernatant and relevant LD density quantification. Scale bars, 50 μm. **(J, K)** Analysis of TG content **(J)** and fluorescence detection of C12-labeled LDs **(K)** after co-culturing with exosomes and functional inhibitors. **(L)** Schematic of HFD mice subcutaneous tumorigenesis model. **(M)** Observation of changes in tumorigenicity in HFD nude mice ($n=5$). **(N)** The tumor weight of the four groups. **(O, P)** Representative IHC images (O) and quantitative analysis **(P)** of Ki67 and PLIN2 staining. Scale bars, 50 μm. $^{*}P<0.05$, $^{**}P<0.01$, $^{***}P<0.001$

by decreasing oxidative phosphorylation [26]. In adipocytes pretreated with H-exo, the ROS level and NADPH/NADP$^{+}$ increased (Fig. S2C, D), further suggesting that adipocytes undergo oxidative stress as a result of exosomes released by hypoxic NPC cells. To reverse the adverse changes in gene profiles caused by oxidative stress in adipocytes, we queried the Connectivity Map database (https://clue.io/) based on the differentially expressed genes in the RNA-seq data (Fig. 4C). Among the selected small-molecule compounds, dicumarol and

buflomedil showed the greatest potential in reversing NADPH/NADP + ratio caused by oxidative stress in adipocytes treated with H-exo (Fig. S2E).

Notably, GSEA confirmed the enrichment of protein secretion (Fig. 4D). Since LD release is an energy-consuming process, we further examined the differential ATPase expression status. The volcano plot showed that 31 ATPases were highly expressed in adipocytes treated with H-exo (Fig. 4E). Based on these findings and the GSEA results, VPS4B was proposed as a key signaling protein involved in LD release, and increased *VPS4B* expression was validated (Fig. 4F). VPS4B is a vesicular trafficking–associated member of the AAA ATPase family associated with diverse cellular activities [27]. It performs a key function in this pathway of disassembling membrane-associated ESCRT-III assemblies, which are vital for forming multivesicular bodies (MVBs), possibly in conjunction with membrane remodeling [27, 28]. We speculate that VPS4B promotes the maturation and release of LDs by forming MVBs. In the LD release experiments, brefeldin A, an inhibitor of protein secretion, and MSC1094308, a VPS4B-allosteric inhibitor, prevented LD release from adipocytes stimulated by H-exo (Fig. 4G–K). In parallel, HFD-fed mice were used to establish subcutaneous tumorigenesis models to directly monitor the role of VPS4B in tumorigenicity (Fig. 4L). H-exo was used to trigger the release of LDs from adipocytes into the TME, intraperitoneal injection of brefeldin A and MSC1094308 consistently reversed tumorigenesis caused by LD accumulation (Fig. 4M–P and Fig. S3A–D). These results suggest that the ATPase VPS4B moderately increased LD release to favor hypoxic NPC growth.

### ANXA5 interacts with VPS4B to enhance cell membrane fluidity

We further assessed whether an interacting protein of VPS4B was involved in LD release. After confirming the efficiency of VPS4B overexpression (Fig. S4A–C), the Co-IP products of the control and VPS4B-overexpression group of adipocytes were subjected to protein sequencing analysis. Functional enrichment analysis identified various functional binding proteins (Fig. 5A). Next, we

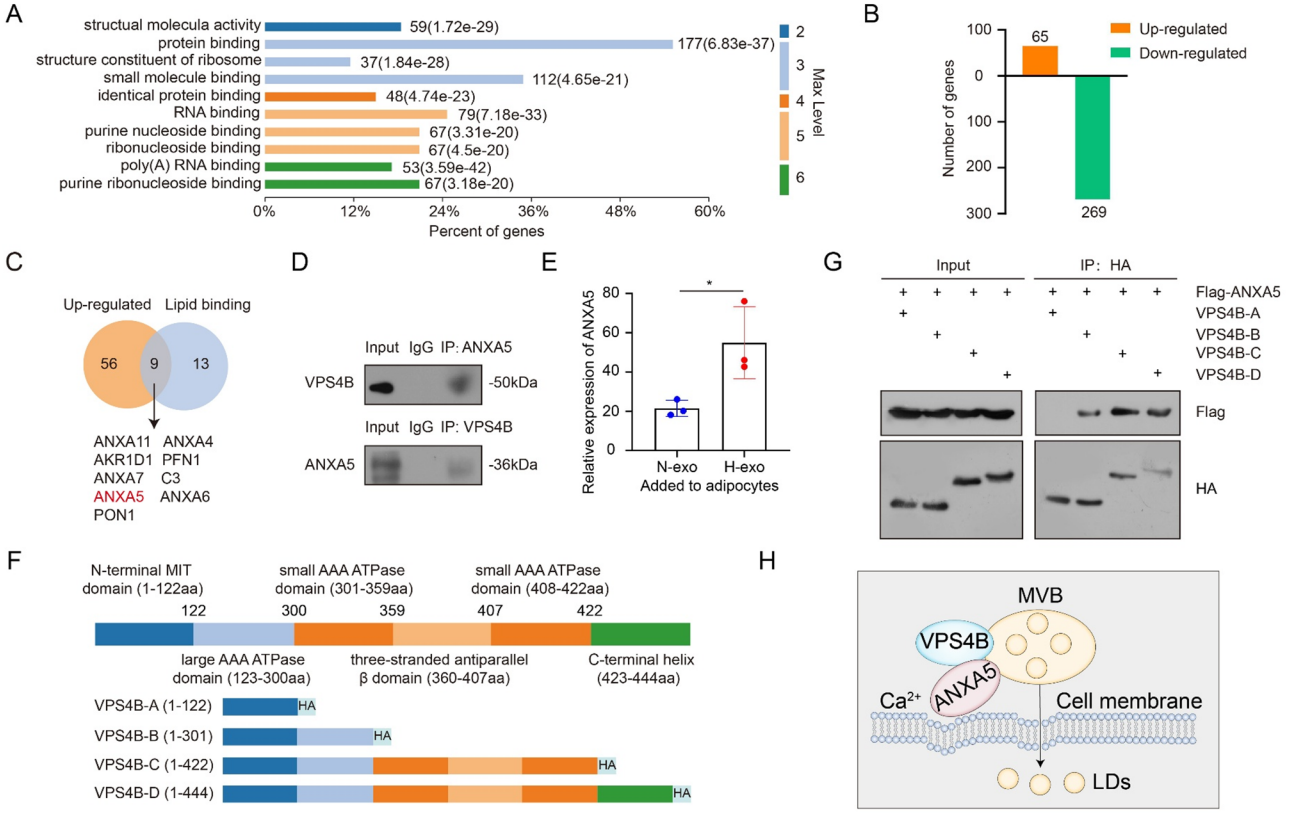


**Fig. 5** ANXA5 binds to the ATPase domain of VPS4B. **(A–C)** Adipocytes were first transfected with lentivirus to overexpress VPS4B, and Co-IP assay combined with mass spectrometry analysis was utilized to screen and identify the immunoprecipitated proteins. **(A)** The functional enrichment analysis of differential genes. **(B)** A comparison of transcription efficiency between genes in the overexpressed VPS4B group and those in the control group. **(C)** Aggregation analysis of genes between up-regulated genes and lipid binding proteins. **(D)** Co-IP analysis between VPS4B and ANXA5 in adipocytes. **(E)** The ANXA5 mRNA expression according to RNA-seq data mentioned in Fig. 4C. **(F, G)** Analysis of ANXA5 binding domains with VPS4B. Various truncated forms of HA-VPS4B **(F)** were individually co-transfected with Flag-ANXA5 into adipocytes, and Co-IP was performed with an anti-HA antibody **(G)**. **(H)** Mechanism diagram of the interaction between VPS4B and ANXA5 in LD release. *$P < 0.05$

conducted an aggregation analysis of lipid-binding proteins and 65 upregulated proteins in the VPS4B-overexpressing group (Fig. 5B, C; Table S1). Interestingly, five annexins were among the enriched proteins. Co-IP assays were also performed (Fig. 5C, D and Fig. S4D), and ANXA5 was identified as an important VPS4B interaction protein. Since ANXA5 is essential for membrane repair and form a protective two-dimensional array at the membrane damage site [29], it may maintain optimal membrane fluidity by recognizing VPS4B. Notably, high ANXA5 expression was observed in the RNA-seq data (Fig. 5E). Since ANXA5 has been found in exosomes from colorectal carcinoma [35], it is reasonable to assume that hypoxic NPC cells might deliver more ANXA5 to adipocytes through exosomes. Consistently, ANXA5 content was higher in hypoxic than in normoxic NPC cell-derived exosomes (Fig. S4E). Moreover, high ANXA5 expression predicted poor prognosis in patients with HNSC (Fig. S4F).

#### VPS4B collaborates with ANXA5 through its ATPase domain to promote LD release, tumor cell proliferation and migration subsequently

Next, to map the specific ANXA5-interacting region in VPS4B, we designed several plasmids with truncated VPS4B and a hemagglutinin (HA) tag, each group of adipocytes was pre-transfected with a Flag-tagged ANXA5 plasmid (Fig. 5F). Co-IP results showed that the small and large AAA ATPase domains of VPS4B, but not the microtubule-interacting and trafficking (MIT) domain, were required for its interaction with ANXA5 (Fig. 5G). These data suggest an intriguing role of VPS4B in LD release by cooperating with ANXA5 via its ATPase domains. In addition, immunofluorescence showed that ANXA5 colocalized with VPS4B in the cytoplasm (Fig. S4G, H). We conducted in vitro cellular experiments to understand the effects of domain binding on LD release. Quantification of LDs in the adipocyte supernatant showed that ANXA5 enhanced LD release, and this effect was amplified in the presence of abundant VPS4B ATPase domains (Fig. S5A, B). Transwell and EdU assays supported a close association between LD content in the conditional media mentioned prior and the malignant phenotypes of NPC cells (Fig. S5C–F). Therefore, the significance of the interaction between ANXA5 and the VPS4B-ATPase domains lies in their roles in LD mature and alterations in cell membrane fluidity.

#### H-exo transmits suppressed LKB1-AMPK signaling to induce VPS4B O-GlcNAc modification for adipocyte LD release

It is well known that LKB1 activates the AMPK pathway in response to metabolic stress [30]. Notably, KEGG analysis showed suppression of AMPK signaling in adipocytes pretreated with H-exo (Fig. 6A and Table S2). We also found that low expression of LKB1 in H-exo transmitted suppressed LKB1-AMPK signaling in adipocytes (Fig. 6B–G). Moreover, VPS4B was predicted to contain numerous O-GlcNAc modification sites (https://services.healthtech.dtu.dk/services/YinOYang-1.2/) (Fig. 6H). Of note, O-GlcNAc modification is an important post-translational protein modification that dynamically regulates intracellular metabolism and signaling pathways [31]. Since glutamine-fructose-6-phosphate amidotransferase (GFAT) is a key enzyme in the HBP [32] (Fig. 6J), and its high expression was observed in adipocytes pretreated with exosomes from hypoxic NPC cells (Fig. 6B) but not in NPC cell-derived exosomes (Fig. 6I), we speculated that adipocytes may undergo HBP metabolic remodeling. It is possible that the suppression of LKB1-AMPK signaling in adipocytes results in the activation of the HBP pathway, leading to an increase in the O-GlcNAc level of VPS4B and an enhancement in the protein stability of VPS4B (Fig. 6J). Therefore, we investigated the effects of O-GlcNAc modification on VPS4B expression in adipocytes. As a result, VPS4B and ANXA5 expression was influenced by HBP flux, with O-GlcNAc modification promoting VPS4B expression (Fig. 6K). These results suggest that the inhibition of LKB1-AMPK signaling leads to the activation of HBP flux in adipocytes.

## Discussion

The complex communication between adipose and tumor tissues supports a parallel evolution model for tumors. Several key factors were identified in the transformation of adipocytes into cancer-associated adipocytes, including peroxisome proliferator-activated receptor gamma (PPARγ) [33]; CCAAT enhancer binding protein alpha (C/EBPα) [34]; lipase E, hormone-sensitive lipase (LIPE/HSL) [35]; and fatty acid binding proteins (FABPs) [36]. In addition, the adipose tissue promotes the formation of pro-inflammatory niches, systemically preconditioning the TME for future metastasis [37]. Our findings extend the concept of lipid metabolism reprogramming. Our analysis shows that adipocytes serve as an energy reservoir to provide a continuous stream of LDs for the malignant biological behavior of NPC cells. In addition, macropinocytosis functioned as a rapid endocytic pathway for LD uptake by NPC cells. These data support the hypothesis that NPC cells induce adipocytes to generate more LDs for energy supply and malignant growth through a symbiotic metabolic relationship.

Extensive research has focused on the role of exosomes in the intercellular communication between tumor cells and adipocytes. Adipocytes were endowed with tumor-promoting properties by exosomes derived from hepatocarcinoma cells [38]. Exosomal long intergenic non-protein coding RNA regulator of reprogramming

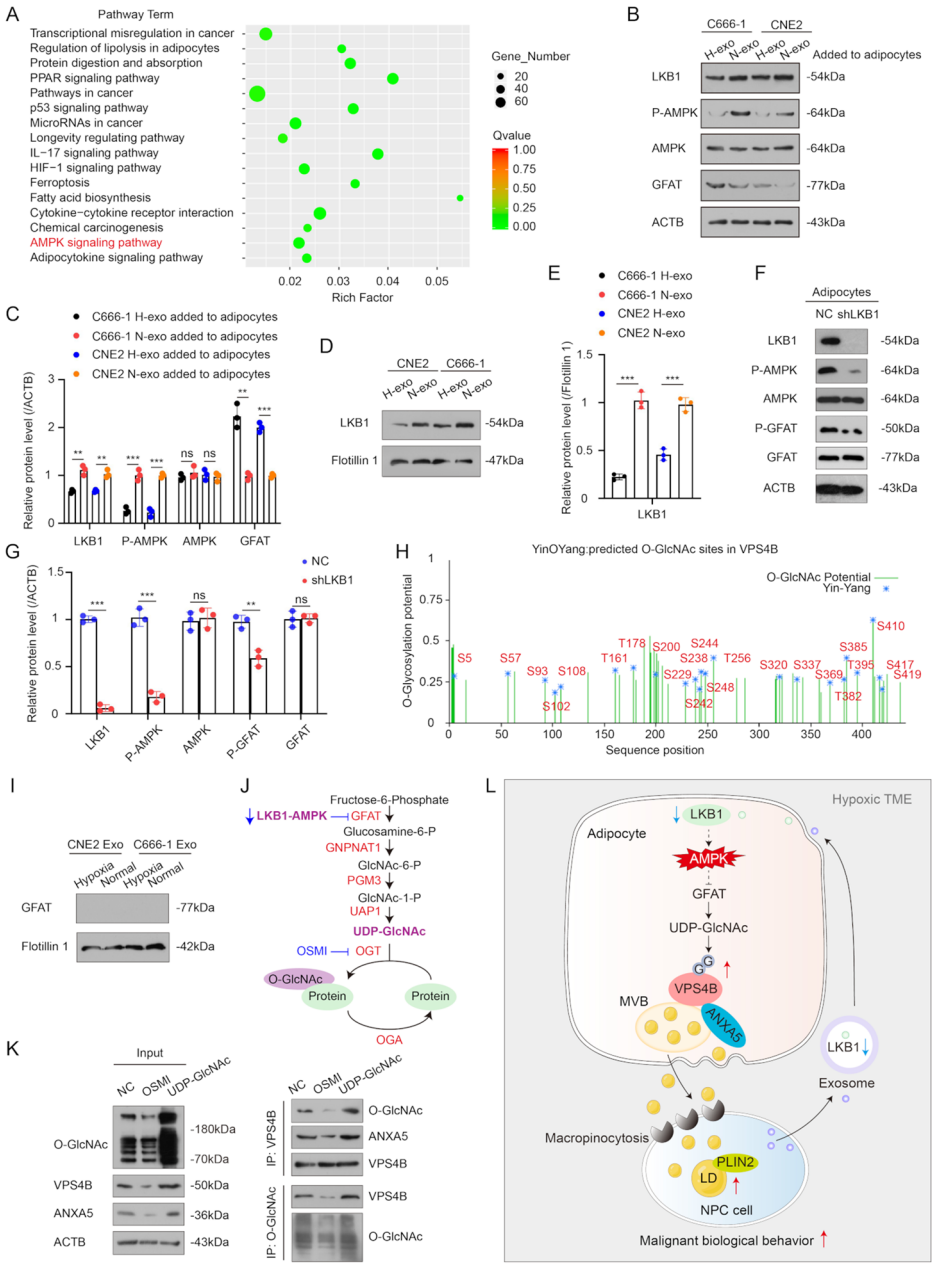


**Fig. 6** H-exo transmits suppressed LKB1-AMPK signaling to induce VPS4B O-GlcNAc modification for adipocyte LD release. **(A)** KEGG analysis of differentially expressed genes in adipocytes based on RNA-seq data from Fig. 4C. Specifically, adipocytes were treated with exosomes derived from normoxic and hypoxic CNE2 cells. **(B, C)** Western blotting detected LKB1, P-AMPK, AMPK and GFAT expression in adipocytes following exosomes added from normoxic and hypoxic NPC cells. **(D, E)** Western blotting analysis of LKB1 in exosomes derived from NPC cells under hypoxia and normoxia. **(F, G)** In adipocytes transfected with NC and shLKB1, Western blotting identified the expression levels of LKB1, P-AMPK, AMPK, P-GFAT, and GFAT. **(H)** The multiple potential O-GlcNAc sites on VPS4B were predicted by YinOYang Database (https://services.healthtech.dtu.dk/services/ YinOYang-1.2/). **(I)** Western blotting experiment represented no GFAT protein expression detected in exosomes derived from NPC cells. **(J)** Schematic diagram of the HBP pathway. GFAT, GNPNAT1 (Glucosamine 6-phosphate N-acetyltransferase), PGM3 (Phosphoacetylglucosamine mutase 3), and UAP1(UDP-N-acetylglucosamine pyrophosphorylase 1) are key enzymes for UDP-GlcNAc synthesis. The dynamic cycling of O-GlcNAc modifications is regulated by OGT (O-GlcNAc transferase) and OGA (O-GlcNAcase). **(K)** After transfection of the OGT inhibitor OSMI and protein glycosylation reactions substrate UDP-GlcNAc, the O-glycosylation level of VPS4B was detected by Co-IP in adipocytes. **(L)** Schematic of the metabolic symbiosis between NPC cells and adipocytes through exosomes and LDs. ns, not significant, $^{**}P < 0.01$, $^{***}P < 0.001$

(LINC-ROR) released by pancreatic cancer cells contributes to the dedifferentiation of adipocytes into fibroblast-like cells, sustaining tumor cell proliferation and migration [39]. Our results demonstrate that H-exo can promote LD release by increasing membrane fluidity in adipocytes. Subsequently, we examined the molecules responsible for altering the fluidity of adipocyte membranes. VPS4B was selected as a candidate because of its possible role in ATP-dependent membrane fission. Suppression of ATPase function by MSC1094308 effectively weakened tumorigenicity in vivo. Several studies have investigated the oncogenic role of VPS4B. VPS4B inactivation reduces the autophagic ability of KPC cells and increases the infiltrative ability of cluster of CD8 + T cells [40]. Additionally, VPS4B functions in the biogenesis of enveloped viruses in an ESCRT III-dependent manner, enabling them to resist antibody-mediated neutralization [41]. Moreover, a strong synthetic lethal dependency exists between VPS4A and VPS4B in cancers with chromosome 18q or 16q deletions [42]. In this study, we found that ANXA5 in hypoxic NPC cell-derived exosomes mainly acts by binding to the ATPase domain of VPS4B. When the ANXA5 and VPS4B ATPase domains were overexpressed, adipocytes tended to release more LDs. Thus, we speculate that VPS4B facilitates LD maturation in adipocytes by promoting the formation of MVBs, transporting LDs to the plasma membrane boundary, and recruits ANXA5 for calcium- and phospholipid-binding, thereby inducing alterations in cell membrane fluidity and expediting LD release (Fig. 5H). The invasive and proliferative abilities of NPC cells were stronger when they absorbed more LDs from the conditioned medium.

Concurrent mutations in KRAS and LKB1 in NSCLC lead to the activation of HBP by GFPT2 [43]. GFPT1 activity is inhibited by AMPK phosphorylation at serine 243 [44]. These results raise the possibility that the direct phosphorylation of key enzymes by AMPK helps regulate HBP metabolic flux. In line with these findings, we demonstrated that GFAT-mediated HBP flux activation via inhibition of LKB1-AMPK signaling is required for VPS4B O-GlcNAc modification. The O-GlcNAc modification maintained the stability of VPS4B, thus facilitating the interaction between ANXA5 and VPS4B for LD release in adipocytes (Fig. 6L). However, as no clinically approved drugs exist that inhibit GFAT in a well-tolerated manner, targeting the HBP flux with other metabolic drugs is worth exploring.

This study is limited by its exclusive focus on LDs from adipocytes, neglecting the significant contributions of neutrophils and macrophages as sources of LDs. Interestingly, cancer cells synthesize more lipid droplets themselves while phagocytose more LDs compared with normal cells. The biological significance of cancer cells phagocytosing LDs in alleviating lipotoxicity, relieving oxidative stress, and obtaining energy deserves more research.

## Conclusions

In this study, we showed that hypoxic NPC cells release exosomes containing LKB1-AMPK inhibitory signals into adipocytes, resulting in the activation of GFAT expression and HBP metabolic flux as well as an increase in the O-GlcNAc levels of VPS4B. Then, VPS4B recruits ANXA5 to induce alterations in cell fluidity and form a cascade of LD release. Ultimately, macropinocytosis of LDs by NPC cells from the TME favored malignant behavior. Our data uncover a new model of metabolic symbiosis between NPC cells and adipocytes, highlighting a promising direction for improving NPC therapy by targeted drug design against VPS4B O-GlcNAc modification.

**Abbreviations**

| | |
|---|---|
| AMPK | AMP-activated protein kinase |
| ANXA5 | Annexin A5 |
| CAAs | Cancer-associated adipocytes |
| CM | Conditioned medium |
| DAB | Diamine benzidine |
| EBV | Epstein–Barr virus |
| EIPA | 5-(N-ethyl-N-isopropyl) amiloride |
| FABPs | Fatty acid binding proteins |
| FASN | Fatty acid synthase |
| FFA | Free fatty acids |
| FRAP | Fluorescence recovery after photobleaching |
| GFAT | Glutamine-fructose-6-phosphate amidotransferase |
| GNPNAT1 | Glucosamine 6-phosphate N-acetyltransferase |
| GSEA | Gene set enrichment analysis |
| HA | Hemagglutinin |
| HBP | Hexosamine biosynthesis pathway |
| H-exo | Hypoxic NPC cell-derived exosome |
| HFD | High-fat diet |
| HIF-1α | Hypoxia-inducible factor 1 subunit alpha |
| HNSC | Head and neck squamous cell carcinoma |
| HPA | Human pre-adipocytes |
| IF | Immunofluorescence |
| IHC | Immunohistochemistry |
| KEGG | Kyoto Encyclopedia of Genes and Genomes |
| LD | Lipid droplet |
| LINC-ROR | Long intergenic non-protein coding RNA regulator of reprogramming |
| LIPE/HSL | Lipase E, hormone-sensitive lipase |
| LMP1 | Latent membrane protein 1 |
| MIT | Microtubule-interacting and trafficking |
| MVBs | Multivesicular bodies |
| NC | Negative control |
| N-exo | Normoxia NPC cell-derived exosome |
| NPC | Nasopharyngeal carcinoma |
| OGA | O-GlcNAcase |
| O-GlcNAc | O-linked N-acetylglucosamine |
| OGT | O-GlcNAc transferase |
| PGM3 | Phosphoacetylglucosamine mutase 3 |
| PLIN2 | Perilipin 2 |
| PPARγ | Peroxisome proliferator-activated receptor gamma |
| PUFA | Polyunsaturated fatty acid |
| STK11/LKB1 | Serine/threonine kinase 11 |
| TCGA | The Cancer Genome Atlas |
| TGs | Triglycerides |
| TME | Tumor microenvironment |
| UAP1 | UDP-N-acetylglucosamine pyrophosphorylase 1 |
| VPS4B | Vacuolar protein sorting 4 homolog B |

## Supplementary Information

The online version contains supplementary material available at https://doi.org/10.1186/s40170-025-00393-3.

Supplementary Material 1

**Acknowledgements**
The authors thank Shanghai Bioprofile Technology Co., Ltd for technical assistance.

**Author contributions**
Conceptualization, B.Y., H.Y., Y.S., and Q.Z.; Methodology, H.Y., L.Y., Q.Z., and F.J.; Software, Y.S.; Validation, Y.H. and R.W.; Formal analysis, T.X. Investigation, K.Z.; Resources, B.Y. and Y.Y.; Data Curation, Y.S. and Q.Z.; Writing - Original Draft, H.Y. and Y.S.; Writing - Review & Editing, B.Y., Y.Y., and Q.Z.; Visualization, H.Y.; Supervision, Y.S. and Y.Y.; Project administration, B.Y.; Funding acquisition, B.Y., Y.Y., Y.S., and H.Y. H.Y., Y.S., and Q.Z. are listed as the co-first authors in recognition of their significant contribution to the inception of this study equally.

**Funding**
This work was supported by grants from National Natural Science Foundation of China (no. 82372977; no. 82173288; no. 82103435; no. 81972554; no. 81602385), Natural Science Foundation of Jiangsu Province (no. BK20201208), Jiangsu Provincial Medical Key Discipline (Laboratory) Cultivation Unit (JSDW202244), Jiangsu Provincial Research Hospital (YJXYY202204), CSCO Clinical Oncology Research Foundation of Beijing (no. Y-HR2019-0463), Postgraduate Research & Practice Innovation Program of Jiangsu Province (no. KYCX23_3429).

**Data availability**
Survival analysis for PLIN2 and HIF-1α synergistically expressed in patients with HNSC was performed using data obtained from the TCGA database ( https://portal.gdc.cancer.gov). The reference data used for the Pearson's correlation analysis of PLIN2 and HIF-1α in NPC is available in the NCBI GEO database under accession code GSE61218. The RNA-seq results were acquired from the NCBI SRA database with the accession number PRJNA1021000. The Connectivity Map database (https://clue.io/) was used to identify potential small-molecule compounds. Information on molecular structures was retrieved from the PubChem database (https://pubchem.ncbi.nlm.nih.gov/). Source data are provided in this study.

## Declarations

**Ethics approval and consent to participate**
All animal experiments were approved by the Committee on Ethics of the Laboratory Animal Center of Nantong University (RDD number: S20230420-007).

**Consent for publication**
All the authors have read and approved the submission of the current version of the manuscript.

**Competing interests**
The authors declare no competing interests.

**Author details**
[1]Department of Otorhinolaryngology Head and Neck Surgery, Affiliated Hospital of Nantong University, Medical School of Nantong University, Nantong 226001, China
[2]Institute of Otolaryngology Head and Neck Surgery, Affiliated Hospital of Nantong University, Nantong 226001, China
[3]Operating Room, Affiliated Hospital of Nantong University, Nantong 226001, China
[4]Department of General, Visceral, Cancer and Transplantation Surgery, University Hospital of Cologne, Cologne, Germany
[5]Department of Radiotherapy, Affiliated Hospital of Nantong University, Nantong 226001, China

Received: 20 November 2024 / Accepted: 5 May 2025
Published online: 23 May 2025

**References**

1. Chen YP, Chan ATC, Le QT, Blanchard P, Sun Y, Ma J. Nasopharyngeal carcinoma. Lancet. 2019;394(10192):64–80.
2. Bossi P, Chan AT, Licitra L, Trama A, Orlandi E, Hui EP, Halámková J, Mattheis S, Baujat B, Hardillo J, et al. Nasopharyngeal carcinoma: ESMO-EURACAN clinical practice guidelines for diagnosis, treatment and follow-up(†). Annals Oncology: Official J Eur Soc Med Oncol. 2021;32(4):452–65.
3. Li L, Tang Q, Ge J, Wang D, Mo Y, Zhang Y, Wang Y, Xiong F, Yan Q, Liao Q, et al. METTL14 promotes lipid metabolism reprogramming and sustains nasopharyngeal carcinoma progression via enhancing m(6)A modification of ANKRD22 mRNA. Clin Transl Med. 2024;14(7):e1766.
4. Zhang P, He Q, Wang Y, Zhou G, Chen Y, Tang L, Zhang Y, Hong X, Mao Y, He Q, et al. Protein C receptor maintains cancer stem cell properties via activating lipid synthesis in nasopharyngeal carcinoma. Signal Transduct Target Ther. 2022;7(1):46.
5. Zhang Y, Pang C, Zhang C, Wang Y, Wang P, Chen Y, Wang J, Hu Y, Liu C, Liang H, et al. HILPDA-mediated lipidomic remodelling promotes radiotherapy resistance in nasopharyngeal carcinoma by accelerating mitophagy. Cell Mol Life Sci. 2023;80(9):242.
6. Zadoorian A, Du X, Yang H. Lipid droplet biogenesis and functions in health and disease. Nat Reviews Endocrinol. 2023;19(8):443–59.
7. Olzmann JA, Carvalho P. Dynamics and functions of lipid droplets. Nat Rev Mol Cell Biol. 2019;20(3):137–55.
8. Cheng X, Geng F, Pan M, Wu X, Zhong Y, Wang C, Tian Z, Cheng C, Zhang R, Puduvalli V, et al. Targeting DGAT1 ameliorates glioblastoma by increasing fat catabolism and oxidative stress. Cell Metabol. 2020;32(2):229–e242228.
9. Yi M, Li J, Chen S, Cai J, Ban Y, Peng Q, Zhou Y, Zeng Z, Peng S, Li X, et al. Emerging role of lipid metabolism alterations in Cancer stem cells. J Exp Clin Cancer Res. 2018;37(1):118.
10. Lo AK, Lung RW, Dawson CW, Young LS, Ko CW, Yeung WW, Kang W, To KF, Lo KW. Activation of sterol regulatory element-binding protein 1 (SREBP1)-mediated lipogenesis by the Epstein-Barr virus-encoded latent membrane protein 1 (LMP1) promotes cell proliferation and progression of nasopharyngeal carcinoma. J Pathol. 2018;246(2):180–90.
11. Liu SC, Tsang NM, Lee PJ, Sui YH, Huang CH, Liu TT. Epstein-Barr virus induces adipocyte dedifferentiation to modulate the tumor microenvironment. Cancer Res. 2021;81(12):3283–94.
12. Snaebjornsson MT, Janaki-Raman S, Schulze A. Greasing the wheels of the Cancer machine: the role of lipid metabolism in Cancer. Cell Metabol. 2020;31(1):62–76.
13. Wei W, Qin B, Wen W, Zhang B, Luo H, Wang Y, Xu H, Xie X, Liu S, Jiang X, et al. FBXW7β loss-of-function enhances FASN-mediated lipogenesis and promotes colorectal cancer growth. Signal Transduct Target Therapy. 2023;8(1):187.
14. Minami JK, Morrow D, Bayley NA, Fernandez EG, Salinas JJ, Tse C, Zhu H, Su B, Plawat R, Jones A, et al. CDKN2A deletion remodels lipid metabolism to prime glioblastoma for ferroptosis. Cancer Cell. 2023;41(6):1048–e10601049.
15. Paskeh MDA, Entezari M, Mirzaei S, Zabolian A, Saleki H, Naghdi MJ, Sabet S, Khoshbakht MA, Hashemi M, Hushmandi K, et al. Emerging role of exosomes in cancer progression and tumor microenvironment remodeling. J Hematol Oncol. 2022;15(1):83.
16. Yin H, Qiu X, Shan Y, You B, Xie L, Zhang P, Zhao J, You Y. HIF-1α downregulation of miR-433-3p in adipocyte-derived exosomes contributes to NPC progression via targeting SCD1. Cancer Sci. 2021;112(4):1457–70.
17. Flaherty SE 3rd, Grijalva A, Xu X, Ables E, Nomani A, Ferrante AW Jr. A lipase-independent pathway of lipid release and immune modulation by adipocytes. Science. 2019;363(6430):989–93.
18. Li P, Lu M, Shi J, Gong Z, Hua L, Li Q, Lim B, Zhang XH, Chen X, Li S, et al. Lung mesenchymal cells elicit lipid storage in neutrophils that fuel breast cancer lung metastasis. Nat Immunol. 2020;21(11):1444–55.
19. You B, Pan S, Gu M, Zhang K, Xia T, Zhang S, Chen W, Xie H, Fan Y, Yao H, et al. Extracellular vesicles rich in HAX1 promote angiogenesis by modulating ITGB6 translation. J Extracell Vesicles. 2022;11(5):e12221.
20. Qiu B, Ackerman D, Sanchez DJ, Li B, Ochocki JD, Grazioli A, Bobrovnikova-Marjon E, Diehl JA, Keith B, Simon MC. HIF2α-Dependent lipid storage promotes Endoplasmic reticulum homeostasis in Clear-Cell renal cell carcinoma. Cancer Discov. 2015;5(6):652–67.

21. Zhou X, Zhang J, Lv W, Zhao C, Xia Y, Wu Y, Zhang Q. The pleiotropic roles of adipocyte secretome in remodeling breast cancer. J Experimental Clin cancer Research: CR. 2022;41(1):203.
22. Kimura I, Ichimura A, Ohue-Kitano R, Igarashi M. Free fatty acid receptors in health and disease. Physiol Rev. 2020;100(1):171–210.
23. Wang G, Heijs B, Kostidis S, Rietjens RGJ, Koning M, Yuan L, Tiemeier GL, Mahfouz A, Dumas SJ, Giera M, et al. Spatial dynamic metabolomics identifies metabolic cell fate trajectories in human kidney differentiation. Cell Stem Cell. 2022;29(11):1580–e15931587.
24. Xie C, Ji N, Tang Z, Li J, Chen Q. The role of extracellular vesicles from different origin in the microenvironment of head and neck cancers. Mol Cancer. 2019;18(1):83.
25. Morigny P, Houssier M, Mairal A, Ghilain C, Mouisel E, Benhamed F, Masri B, Recazens E, Denechaud PD, Tavernier G, et al. Interaction between hormone-sensitive lipase and ChREBP in fat cells controls insulin sensitivity. Nat Metabolism. 2019;1(1):133–46.
26. Tang K, Zhu L, Chen J, Wang D, Zeng L, Chen C, Tang L, Zhou L, Wei K, Zhou Y, et al. Hypoxia promotes breast Cancer cell growth by activating a glycogen metabolic program. Cancer Res. 2021;81(19):4949–63.
27. Stuchell-Brereton MD, Skalicky JJ, Kieffer C, Karren MA, Ghaffarian S, Sundquist WI. ESCRT-III recognition by VPS4 ATPases. Nature. 2007;449(7163):740–4.
28. Tseng CC, Dean S, Davies BA, Azmi IF, Pashkova N, Payne JA, Staffenhagen J, West M, Piper RC, Odorizzi G, Katzmann DJ. Bro1 stimulates Vps4 to promote intralumenal vesicle formation during multivesicular body biogenesis. J Cell Biol 2021, 220(8).
29. Mularski A, Sønder SL, Heitmann ASB, Nylandsted J, Simonsen AC. Simultaneous membrane binding of Annexin A4 and A5 suppresses 2D lattice formation while maintaining curvature induction. J Colloid Interface Sci. 2021;600:854–64.
30. Kottakis F, Bardeesy N. LKB1-AMPK axis revisited. Cell Res. 2012;22(12):1617–20.
31. Yang X, Qian K. Protein O-GlcNAcylation: emerging mechanisms and functions. Nat Rev Mol Cell Biol. 2017;18(7):452–65.
32. Chatham JC, Zhang J, Wende AR. Role of O-Linked N-Acetylglucosamine protein modification in cellular (Patho)Physiology. Physiol Rev. 2021;101(2):427–93.
33. Broekema MF, Massink MPG, Donato C, de Ligt J, Schaarschmidt J, Borgman A, Schooneman MG, Melchers D, Gerding MN, Houtman R, et al. Natural helix 9 mutants of PPARγ differently affect its transcriptional activity. Mol Metabolism. 2019;20:115–27.
34. Sabatier M, Birsen R, Lauture L, Mouche S, Angelino P, Dehairs J, Goupille L, Boussaid I, Heiblig M, Boet E, et al. C/EBPα confers dependence to fatty acid anabolic pathways and vulnerability to lipid oxidative Stress-Induced ferroptosis in FLT3-Mutant leukemia. Cancer Discov. 2023;13(7):1720–47.
35. Das SK, Eder S, Schauer S, Diwoky C, Temmel H, Guertl B, Gorkiewicz G, Tamilarasan KP, Kumari P, Trauner M, et al. Adipose triglyceride lipase contributes to cancer-associated cachexia. Science. 2011;333(6039):233–8.
36. Li B, Hao J, Zeng J, Sauter ER. SnapShot: FABP functions. Cell. 2020;182(4):1066–e10661061.
37. Bouche C, Quail DF. Fueling the tumor microenvironment with Cancer-Associated adipocytes. Cancer Res. 2023;83(8):1170–2.
38. Wang S, Xu M, Li X, Su X, Xiao X, Keating A, Zhao RC. Exosomes released by hepatocarcinoma cells endow adipocytes with tumor-promoting properties. J Hematol Oncol. 2018;11(1):82.
39. Sun Z, Sun D, Feng Y, Zhang B, Sun P, Zhou B, Du L, Wang Y, Fan Z, Yang J, et al. Exosomal linc-ROR mediates crosstalk between cancer cells and adipocytes to promote tumor growth in pancreatic cancer. Mol Therapy Nucleic Acids. 2021;26:253–68.
40. Frey N, Tortola L, Egli D, Janjuha S, Rothgangl T, Marquart KF, Ampenberger F, Kopf M, Schwank G. Loss of Rnf31 and Vps4b sensitizes pancreatic cancer to T cell-mediated killing. Nat Commun. 2022;13(1):1804.
41. Feng Z, Hensley L, McKnight KL, Hu F, Madden V, Ping L, Jeong SH, Walker C, Lanford RE, Lemon SM. A pathogenic picornavirus acquires an envelope by hijacking cellular membranes. Nature. 2013;496(7445):367–71.
42. Neggers JE, Paolella BR, Asfaw A, Rothberg MV, Skipper TA, Yang A, Kalekar RL, Krill-Burger JM, Dharia NV, Kugener G, et al. Synthetic lethal interaction between the ESCRT paralog enzymes VPS4A and VPS4B in cancers harboring loss of chromosome 18q or 16q. Cell Rep. 2021;36(2):109367.
43. Kim J, Lee HM, Cai F, Ko B, Yang C, Lieu EL, Muhammad N, Rhyne S, Li K, Haloul M, et al. The hexosamine biosynthesis pathway is a targetable liability in KRAS/LKB1 mutant lung cancer. Nat Metab. 2020;2(12):1401–12.
44. Gélinas R, Mailleux F, Dontaine J, Bultot L, Demeulder B, Ginion A, Daskalopoulos EP, Esfahani H, Dubois-Deruy E, Lauzier B, et al. AMPK activation counteracts cardiac hypertrophy by reducing O-GlcNAcylation. Nat Commun. 2018;9(1):374.


## Publisher's note